Transport properties of magnetic tunnel junctions with Co_2MnSi electrodes: The influence of temperature-dependent interface magnetization and electronic band structure

J. Schmalhorst,* A. Thomas, S. Kämmerer, O. Schebaum, D. Ebke, M. D. Sacher, and G. Reiss
Thin Films and Nano Structures, Department of Physics, Bielefeld University, 33501 Bielefeld, Germany

A. Hütten
Institute for Nano-Technology, Research Center Karlsruhe, 76021 Karlsruhe, Germany

A. Turchanin and A. Gölzhäuser
Department of Physics, Bielefeld University, 33501 Bielefeld, Germany

E. Arenholz
Lawrence Berkeley National Laboratory, Berkeley, California 94720, USA
(Received 20 April 2006; revised manuscript received 25 September 2006; published 4 January 2007)

The transport properties of $Co_2MnSi/AlO_x/Co$-Fe magnetic tunnel junctions showing a tunnel magnetoresistance of 95% at low temperatures are discussed with respect to temperature-dependent magnetic moments at the Co_2MnSi/AlO_x interface and electronic band structure effects. These junctions show a considerably larger temperature and bias voltage dependence of the tunneling magnetoresistance compared to Co-Fe-B$/AlO_x/$Co-Fe-B junctions, although the effective spin polarization of Co_2MnSi (66%) is larger than Co-Fe-B (60%). Especially, the tunnel magnetoresistance of the Co_2MnSi based junctions becomes inverse for large bias voltages. With increasing atomic disorder of the interfacial Co_2MnSi its magnetic moments decrease and show a stronger temperature dependence. Even for the best atomic ordering achieved the corresponding spin-wave parameters of Mn and Co at the Co_2MnSi/AlO_x interface are significantly larger than expected for Co_2MnSi bulk and also larger than the spin-wave parameters of Co and Fe at a Co-Fe-B$/AlO_x$ interface. The influence of enhanced interfacial magnon excitation in the $Co_2MnSi/AlO_x/$Co-Fe junctions on their transport properties will be discussed as well as possible origins for the negative tunnel magnetoresistance at high bias voltages.

DOI: 10.1103/PhysRevB.75.014403 PACS number(s): 75.70.−i, 85.75.−d, 78.70.Dm

I. INTRODUCTION

Magnetic tunnel junctions (MTJs) consisting of ferromagnetic electrodes separated by a thin insulating tunnel barrier are promising candidates for sensors, nonvolatile memories and programmable logic devices.[1,2] Their tunnel magnetoresistance (TMR) is desired to be as large as possible and is linked to the Julliére spin polarization[3] $P_{1,2}$ of electrode 1 and 2 by $TMR=2P_1P_2/(1-P_1P_2)$. Currently, giant TMR amplitudes of up to 355% at room temperature (RT) are achieved[4] by substituting the amorphous AlO_x barrier by crystalline MgO and by using $Co_{40}Fe_{40}B_{20}$ electrodes ($P_{Co40Fe40B20}=86\%$ at 5 K).[4] Coherent spin-polarized tunneling, where the symmetries of the electron wave functions are essential, can account for this high effective polarization. The ultimate magnetoelectronic material, a ferromagnetic half-metal, will have a gap in the minority (or majority) electron density of state at the Fermi energy E_F and thus 100% spin polarization. This property has been predicted theoretically for the Heusler alloy Co_2MnSi.[5] Recently, we have prepared $Co_2MnSi/AlO_x/Co_{70}Fe_{30}$ junctions showing a TMR of 95% at 1 mV/20 K,[6] which corresponds to 66% spin polarization of Co_2MnSi. An *in-situ* annealing procedure applied after barrier formation and before depositing the top electrode of the junction has been developed to obtain atomic ordering of the (110) textured Co_2MnSi thin films[7] resulting in the high spin polarization for Co_2MnSi. Recently, Oogane *et al.*[8] have found 89% spin polarization at 1 mV/2 K for *epitaxial* Co_2MnSi electrodes grown in the (100) orientation.

Here we compare the temperature and bias voltage dependent TMR of our Co_2MnSi based junctions with $Co_{62}Fe_{26}B_{12}/AlO_x/Co_{62}Fe_{26}B_{12}$ junctions (showing up to 114% TMR) and $Co_{70}Fe_{30}/AlO_x/Ni_{80}Fe_{20}$ junctions (71%). The influence of the temperature-dependent magnetic moments at the lower electrode/barrier interfaces as well as electronic band structure effects will be addressed. The discussion part of this paper is organized as follows: First, we present an overview of the transport properties of all junctions in Sec. III A to show up the specific characteristics of the Co_2MnSi based MTJs. Afterwards, these junctions are extensively characterized by x-ray absorption and photoemission techniques. The chemical states and the temperature-dependent magnetic moments of Si as well as Co and Mn near the Co_2MnSi/AlO_x interface are discussed in Secs. III B and III C, respectively. The magnetic properties will be compared with those of Co-Fe-B$/AlO_x$ based junctions in Sec. III D. Differences in the electronic band structure between ordered and disordered Co_2MnSi are analyzed in Sec. III E. Finally, the special transport properties of the Co_2MnSi based junctions are discussed in Sec. III F with respect to their chemical and temperature-dependent interface properties.

II. EXPERIMENT

The MTJs were deposited at room temperature by dc- and rf-magnetron sputtering on thermally oxidized Si(100) wafers. To probe the chemical, electronic and magnetic properties at the lower electrode/barrier interface, we prepared three layer stacks, which correspond only to the bottom electrode of our MTJs including the barrier. The bottom electrode of our $Co_2MnSi/AlO_x/Co_{70}Fe_{30}$ junctions consists of oxidized Si-wafer/$V^{42\ nm}/Co_2MnSi^{100\ nm}/Al^{1.4\ nm}$+oxidation. The first stack "CMS100" was *in-situ* annealed at about 450 °C for 40 min immediately after Al oxidation, the second stack "CMS100ag" was kept in the as-grown state, it was not annealed.

The bottom electrode "CoFeB" of the $Co_{62}Fe_{26}B_{12}/AlO_x/Co_{62}Fe_{26}B_{12}$ junction consists of oxidized

$$\text{Si-wafer/Ta}^{5\ nm}\text{/Cu}^{30\ nm}\text{/Ta}^{5\ nm}\text{/Cu}^{5\ nm}\text{/}$$

$$\text{Mn}_{83}\text{Ir}_{17}{}^{12\ nm}\text{/Co}_{62}\text{Fe}_{26}\text{B}_{12}{}^{4\ nm}\text{/Al}^{1.2\ nm}+\text{oxidation},$$

it was *ex-situ* annealed at 275 °C.

To investigate the transport properties of complete junctions, top electrodes were added to stack "CMS100," "CMS100ag," and "CoFeB." In the case of Co_2MnSi-based MTJs the top electrode is $Co_{70}Fe_{30}{}^{5\ nm}/Mn_{83}Ir_{17}{}^{10\ nm}/Al$ $-Ta^{6\ nm}/Cu^{40\ nm}/Ta^{6\ nm}/Au^{20\ nm}$. For the Co-Fe-B based junctions the top electrode is $Co_{52}Fe_{26}B_{12}{}^{4\ nm}/Ni_{81}Fe_{19}{}^{3\ nm}/Ta^{5\ nm}/Cu^{20\ nm}/Au^{30\ nm}$. After deposition all complete MTJ stacks were vacuum annealed *ex-situ* at 275 °C in a magnetic field of 0.1 T to set the exchange bias of the pinned electrode. Subsequently, quadratic junctions with area size $S_J=10\,000-90\,000\ \mu m^2$ were patterned by optical lithography and ion beam etching. The transport properties of the junctions were measured as a function of magnetic field, bias voltage and temperature by conventional two-probe dc and ac techniques.

Additionally, we compare these MTJs to Co $-Fe/AlO_x/Ni-Fe$ junctions ("MTJ-NiFe," Si-wafer/$Cu^{30\ nm}/Ni_{80}Fe_{20}{}^{4\ nm}/Mn_{83}Ir_{17}{}^{15\ nm}/Co_{70}Fe_{30}{}^{3\ nm}/Al^{1.4\ nm}$ +oxidation/$Ni_{80}Fe_{20}{}^{4\ nm}/Ta^{3\ nm}/Cu^{55\ nm}/Au^{20\ nm}$, the Ni-Fe and Co-Fe electrodes are polycrystalline), which have been investigated in detail in Ref. 9.

Temperature-dependent x-ray absorption spectroscopy (XAS) and x-ray magnetic circular dichroism (XMCD) were performed at beamline 4.0.2 of the Advanced Light Source, Berkeley, USA. The Co-, Fe-, and Mn-*L* edges and the Si *-K* edge were investigated. Surface-sensitive total electron yield (TEY)[10] and bulk-sensitive fluorescence yield (FY) spectra[10] were recorded simultanously. The x-ray angle of incidence was 30° to the sample surface. XMCD spectra were obtained by applying a magnetic field (max±0.55 T) along the x-ray beam direction using elliptically polarized radiation with a polarization of 90%. I^+ and I^- denotes spectra for parallel and antiparallel orientation of photon spin and magnetic field. XAS intensity and XMCD effect are defined as $(I^++I^-)/2$ and (I^+-I^-), respectively.

Monochromated Al-K_α x-ray photoelectron spectroscopy (XPS, photon energy 1486.7 eV) was performed to investigate the valence band of Co_2MnSi and to determine the binding energies of the Co-2*p* electrons. The electron emission angle was 20° to the surface normal.

The experimental results are compared to band structure calculations for perfectly $L2_1$-ordered Co_2MnSi bulk material (lattice constant 0.565 nm) obtained using the SPR-KKR program package[11].

III. EXPERIMENTAL RESULTS AND DISCUSSION

As a motivation for the following characterization of the lower electrode–barrier interface by XAS, XMCD, and XPS, we present an overview on the temperature and bias voltage-dependent transport properties first.

A. Transport properties

The low temperature TMR majorloops of "CMS100" and "CMS100ag" MTJs are shown in Fig. 1(a). The *in-situ* annealed sample ("CMS100") shows up to 95% TMR at 20 K/1 mV and a sharp magnetization reversal of the Co_2MnSi around zero magnetic field. Without *in-situ* annealing ("CMS100ag") the TMR is strongly reduced to maximal 1.3% at 16 K/20 mV (±2000 Oe field range). The Co_2MnSi electrode shows superparamagnetic behavior and is not saturated at ±2000 Oe. The pinned Co-Fe top electrode of both samples shows an exchange bias of about −650 Oe. The TMR amplitude of 95% found in the *in-situ* annealed sample "CMS100" corresponds to effective spin polarizations of $P_{Co2MnSi}=66\%$ assuming $P_{Co70Fe30}=49\%$.[6] The maximum TMR of the "CoFeB" junctions is 114% ($P_{Co62Fe26B12}=60\%$) These TMR effects are significantly higher than for conventional Co-Fe/AlO_x/Ni-Fe junctions ["MTJ-NiFe,"

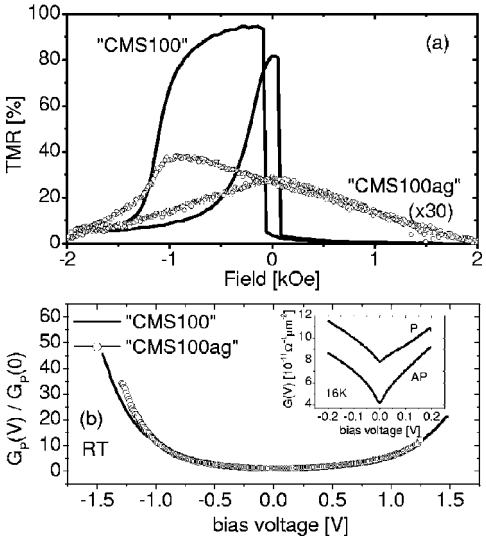

FIG. 1. (a) TMR majorloops for "CMS100" (measured at 20 K/1 mV bias) and "CMS100ag" (16 K/20 mV) based MTJs. (b) Typical differential conductance $G_p=dj/dU$ of both samples measured at RT in the parallel state. The inset shows the typical zero-bias anomaly in the differential conductance *G* of a "CMS100" junction at low temperature for antiparallel (AP) and parallel (P) alignment of the Co_2MnSi and the Co-Fe electrodes.

71% TMR (Ref. 9)]. For the Co_2MnSi based junctions we found minimal area resistance products $R_{min}=13.3$ GΩ μm^2 ("CMS100") and 2.9 GΩ μm^2 ("CMS100ag"), respectively, and very similar tunneling characteristics in the parallel state [see Fig. 1(b)]. But these R_{min} values are much higher than for "CoFeB" (12.5 MΩ μm^2) and "MTJ-NiFe" (32 MΩ μm^2). The low temperature bias voltage dependence (±500 mV range) of the junctions is shown in Fig. 2(a). "CMS100" shows a considerably stronger bias voltage dependence than "Co-Fe-B" and "MTJ-NiFe." The same holds for the temperature dependence of the TMR [Fig. 2(b)], which is identical for MTJs "Co-Fe-B" and "MTJ-NiFe," although their maximum TMR amplitudes are significantly different. Especially, their TMR(T) curves are concave. In contrast, the Co_2MnSi based junction show a convex TMR(T) dependence. Please note, that such a convex TMR(T) dependence is also found by Oogane *et al.*[8] for junctions with *epitaxial* Co_2MnSi electrodes. Our "CMS100ag" junctions prepared without *in-situ* annealing at 450 °C show no TMR above 200 K (the noise level of the TMR measurements was about 0.05%). As usually observed, all junctions show small zero-bias anomalies, which are stronger for antiparallel alignment of the electrodes. An example is shown in the inset of Fig. 1(b) for the MTJ "CMS100."

Remarkably, the *in-situ* annealed junctions "CMS100" show an *inversed* TMR of up to −6.3% at room temperature for large negative bias voltage, i.e., when the electrons are tunneling *from the Co-Fe into the* Co_2MnSi electrode (see Fig. 3). For positive bias voltage, when the electrons are tunneling *from* Co_2MnSi *into Co-Fe*, the TMR remains positive. Please note, that we observed the inversed TMR effect at room temperature as well as at 20 K and that there is a kink in the TMR bias voltage dependence at around −300 mV bias (see arrow in Fig. 3). This inversion of the TMR is not observed for the other three junction types. Their monotonic decrease of the positive TMR with increasing bias voltage shown in Fig. 2 for the ±500 mV bias voltage range just goes on up to the dielectric breakdown of the junctions. For example, the Co-Fe/AlO_x/Ni-Fe junctions[9] "MTJ-NiFe" still show a room temperature TMR of about +10% for ±1200 mV bias voltage. For "CMS100ag" junctions, which were not *in-situ* annealed during layer deposition, the TMR at 16 K is +0.2% for ±1200 mV bias voltage.

Before we discuss these results in Sec. III F, we focus on the chemical, magnetic and electronic properties at the Co_2MnSi-AlO_x interface first in the following sections.

B. Chemical and magnetic properties of Si near the Co_2MnSi/AlO_x interface in Co_2MnSi based junctions

The surface sensitive XAS spectra in TEY detection at the Si-*K* edge of the two samples with Co_2MnSi electrode show two overlapping peaks 8 eV ("Si-1" in Fig. 4) and 6 eV ("Si-2" in Fig. 4) above the Fermi energy E_F. The energetic position of peak "Si-1" is characteristic for SiO_2.[12]. Peak "Si-2" is considerably larger for "CMS100" than for "CMS100ag." This peak can be reproduced by band structure calculations using the SPR-KKR code.[11] It corresponds

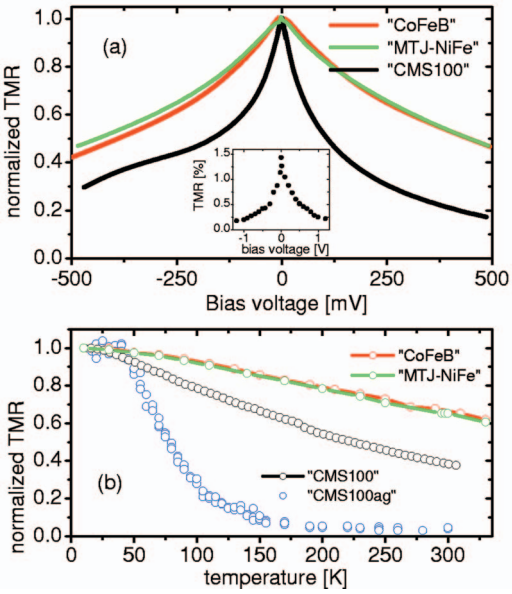

FIG. 2. (Color) (a) Typical bias voltage dependence at low temperature for "CMS100" (measured at 20 K), and "CoFeB" (30 K) and for "MTJ-NiFe" (10 K). All data is normalized to the maximum TMR at low bias. The inset shows the TMR amplitude for "CMS100ag" (16 K) (b) Typical normalized temperature dependence of "CMS100" (measured at 10 mV), "CoFeB" (10 mV), "MTJ-NiFe" (10 mV) and "CMS100ag" (20 mV).

to a small maximum in the density of unoccupied *p*-like Si states about 6 eV above the Fermi energy E_F. Furthermore, the Si-*K* edge spectrum of "CMS100" shows a pronounced x-ray absorption near-edge fine structure (XANES, see black arrows in Fig. 4). This indicates atomic ordering of Co_2MnSi at the lower barrier interface during the *in-situ* annealing at

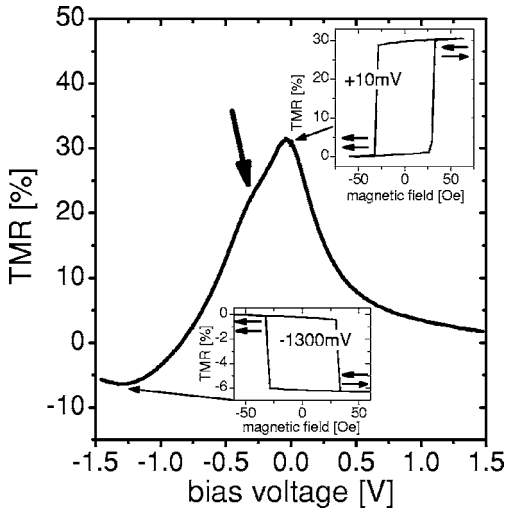

FIG. 3. Typical bias voltage dependence in the ±1500 mV bias voltage range of a "CMS100" junction, measured at room temperaure. The insets show TMR minor loops measured at +10 mV and −1300 mV, when only the magnetization of the soft Co_2MnSi electrode is switched by the external magnetic field. The magnetizations of Co_2MnSi and Co-Fe are aligned parallel (antiparallel) for magnetic fields of −60 Oe (+60 Oe).

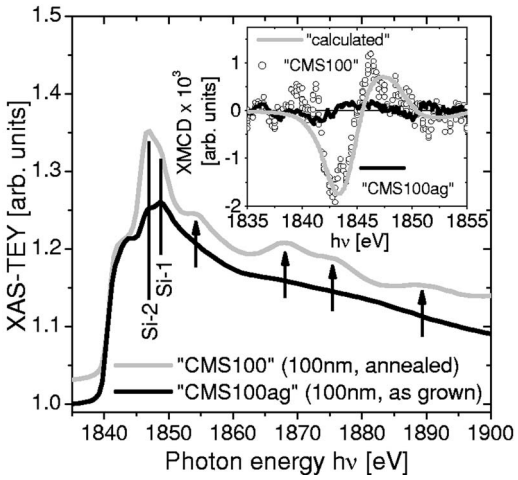

FIG. 4. XAS-TEY spectra at Si-K edge of the annealed sample "CMS100" (gray curve, measured at 15 K) and of the as-grown sample "CMS100ag" (black curve, measured at 300 K). The inset shows the according XMCD asymmetries of both samples and the XMCD asymmetry calculated by the SPR-KKR code (Ref. 11).

450 °C. These fingerprints of the atomic ordering of the Co_2MnSi are correlated to the bulk magnetization of the samples: Only after *in-situ* annealing a room temperature magnetic moments of $4.4\mu_B$ per formula unit is found, which is close to the expected value of nearly $5\mu_B$[13]. Here each Co, Mn, and Si atom contributes with a calculated spin magnetic moment of $1.02\mu_B$ (2×), $2.97\mu_B$, and $-0.074\mu_B$ to the magnetization of the Co_2MnSi.[13] The clear Si-XMCD signal (inset in Fig. 4) found for the annealed "CMS100" is not present in the disordered as-grown sample "CMS100ag." Its shape is in agreement with the calculated[11] XMCD asymmetry corresponding to a tiny Si orbital moment of about $0.002\mu_B$ oriented in parallel to the Mn and Co spin magnetic moments, but it is about two times larger than expected.

C. Chemical and magnetic properties of Co and Mn near the Co_2MnSi/AlO_x interface in Co_2MnSi based junctions

The chemical properties of Co and Mn were also probed by x-ray absorption spectroscopy. In XAS saturation effects[10] occur, if the x-ray penetration depth is not large compared with the information depth of the detected signal. In first order they can be neglected in our TEY spectra, but

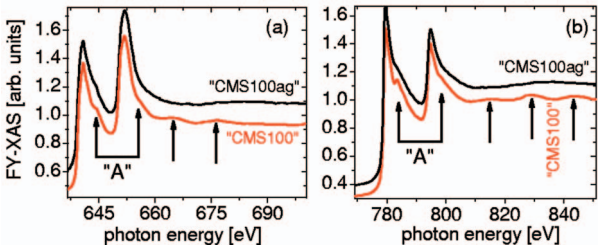

FIG. 5. (Color) XAS-FY spectra at (a) Mn- and (b) Co-L edge of "CMS100ag" and "CMS100." The spectra were measured at 15 K. The XANES oscillations found for the annealed "CMS100" are marked by arrows and are also visible at 300 K.

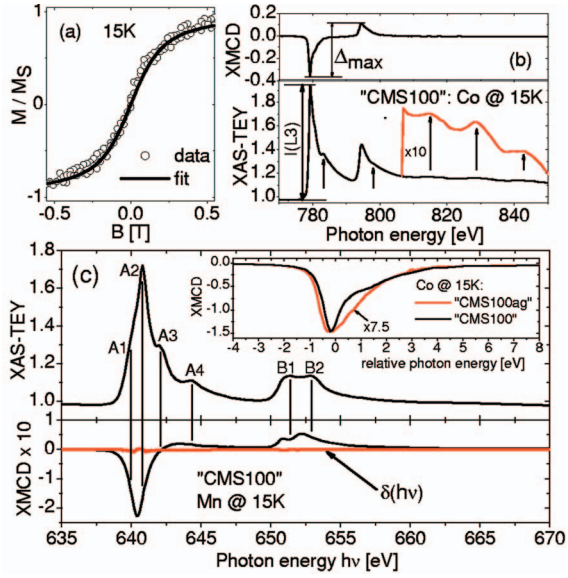

FIG. 6. (Color) (a) Magnetization loop of the as-grown sample "CMS100ag" measured at 15 K (open circles). The black line is a fit by the Langevin function (see text). (b) X-ray absorption spectra and magnetic circular dichroism in TEY mode at the Co-L edge of "CMS100" measured at 15 K. (c) X-ray absorption spectra and magnetic circular dichroism in TEY mode at the Mn-L edge of "CMS100" measured at 15 K. The red curve $\delta(h\nu)$ is the difference of the Mn XMCD asymmetries of "CMS100" measured at 15 K and 300 K, respectively. The inset shows differences of the Co XMCD asymmetry at 15 K between the ordered and disordered sample "CMS100" and "CMS100ag," the photon energy is defined with respect to the energy position of maximum intensity of the Co-L_3 resonance.

reduce the intensities of the $L_{2,3}$ resonances in the bulk sensitive Co and Mn FY spectra shown in Fig. 5. However, pronounced XANES oscillations indicating the atomic ordering throughout the Co_2MnSi layers are found for the annealed sample "CMS100" (see Fig. 5). Additionally, this sample shows shoulders at about 4 eV above the maximum intensities of the Mn- and Co-$L_{2,3}$ resonances (marked by "A" in Fig. 5) which are not present for "CMS100ag." These shoulders reflect small peaks in the density of unoccupied d-like states[11] of the ordered Co_2MnSi. The TEY spectra probing the Co_2MnSi/AlO_x interface show these fingerprints of the atomic ordering in the annealed sample "CMS100" only for Co [see arrows in Fig. 6(b)]. In addition to interfacial SiO_2, MnO identified by its characteristic XAS multiplett structure[14] [see peaks "A1"–"B2" in Fig. 6(c)] is present at the interface for both samples and masks the fingerprints of ordering for interfacial Mn in sample "CMS100." Although the saturation effects change the shape of the bulk sensitive Mn FY spectra shown in Fig. 5(a), it is obvious that the MnO multiplet structure is not present in the Mn FY spectra.

The temperature dependence of the interfacial magnetic moments of Co and Mn is adressed now. For these atoms the magnetic moments are governed by the 3d electrons which can be probed by x-ray absorption at the $L_{2,3}$ edges. By using the total XMCD asymmetry Δ_{max} and the maximal L_3 inten-

sity $I(L3)$ as shown in Fig. 6(b) the normalized total XMCD asymmetry can be defined as $\kappa \equiv \Delta_{max}/I(L3)$, κ is proportional to the element specific magnetic moments. The largest normalized total XMCD asymmetries is found for "CMS100," which also has a high room temperature bulk magnetization of 4.4 μ_B per formula unit: At 15 K $\kappa_{Co,15\ K}=49\%$ is found for Co and $\kappa_{Mn,15\ K}=39\%$ for Mn. According to the XMCD sum rules[15] (spin magnetic dipole term $<T_Z>$ neglected, 2.24 Co-3d holes, 4.52 Mn-3d holes[16]) these XMCD asymmtries correspond to a ratio of the spin magnetic moments m_s^{Mn} for Mn and m_s^{Co} for Co of $m_s^{Mn}/m_s^{Co}=1.4-2.1$. The large uncertainty of this value results from the not precisely known factor to correct the jj mixing for Mn[17]. However, this value is significantly smaller than $m_s^{Mn}/m_s^{Co}=2.9$ as expected from band structure calculations.[13] The reduced magnetic moment ratio is reasonable, because of the Mn-O formation at the interface.

Compared to "CMS100" the magnetic moments of the as-grown sample "CMS100ag" are considerably smaller: The magnetization loop [Fig. 6(a)] calculated[18] from its Co and Mn XMCD asymmetries in TEY mode shows a typical superparamagnetic behavior. By fitting the data with the Langevin function[19] $M/M_S=\coth(\mu_{(T)}B/kT)-(kT/\mu_{(T)}B)$ the mean magnetic moment of the superparamagnetic clusters can be estimated to be $\mu_{(15\ K)}=300\mu_B$ at 15 K. For applied fields of ±0.55 T the normalized total XMCD asymmetry, being proportional to the element specific magnetic moment, is $\kappa_{Co,15\ K}=7.2\%$ for Co and $\kappa_{Mn,15\ K}=4.2\%$ for Mn. These values are reduced at 300 K by a factor of 14.0±1.3 for Co and 13.5±0.9 for Mn, respectively. If $\mu_{(T)}$ was temperature independent, the Langevin function would result in a reduction of $\kappa_{Co/Mn,15\ K}$ by a factor of eight. Therefore, the mean magnetic moments of the clusters themselves are reduced by a factor of 1.8, when the temperature increases from 15 K to 300 K. Especially, the ratio of the Co and Mn XMCD asymmetries is larger for the as grown sample "CMS100ag" ($\kappa_{Co,15\ K}/\kappa_{Mn,15\ K}=1.7$) than for the annealed "CMS100" ($\kappa_{Co,15\ K}/\kappa_{Mn,15\ K}=1.26$). That means, compared to the ordered sample "CMS100" the Mn magnetic moments of "CMS100ag" are further reduced. This is reasonable, because the exchange interaction between neighboring atoms is ferromagnetic for Co-Co and Mn-Co and antiferromagnetic for Mn-Mn[20]. The latter pairs are not present in perfectly ordered Co_2MnSi. But the Mn-Mn coupling pairs exist in the disordered sample "CMS100ag." These might destabilize the ferromagnetic order in the individual grain, reduce the relative magnetic moment of Mn with respect to Co and reduce the exchange interaction across the grain boundaries resulting in the superparamagnetic behavior of the sample.

The temperature dependence of the interfacial magnetic moments of the ordered sample "CMS100" is much smaller than for "CMS100ag." For "CMS100" the magnetic moments of Co and Mn are reduced to 94% and 90% of the low temperature values $\kappa_{Co,15\ K}=49\%$ and $\kappa_{Mn,15\ K}=39\%$, respectively. Assuming a Bloch-like temperature dependence of the interfacial magnetic moments, $m(T)/m(0)=(1-\alpha T^{3/2})$, this corresponds to spin-wave parameters α of $1.17\times10^{-5}\ K^{-3/2}$ for Co and $1.95\times10^{-5}\ K^{-3/2}$ for Mn. These values are 4 (Co) and 6.7 (Mn) times larger than the spin-wave parameter $\alpha_{bulk}=2.81\pm0.21\times10^{-6}\ K^{-3/2}$ of bulk Co_2MnSi measured by Ritchie *et al.*[21]

Please note, that the *spectral shape* of the x-ray absorption spectra and the magnetic circular dichroism asymmetry in TEY detection does not change with temperature for Co and Mn. For Mn, this is shown in Fig. 6(c): The maximal difference $\delta(h\nu)$ $[\equiv XMCD(h\nu)_{300\ K}\times\Delta_{max,15\ K}/\Delta_{max,300\ K}-XMCD(h\nu)_{15\ K}$, with photon energy $h\nu$] of the energy-dependent Mn XMCD asymmetries of the annealed sample "CMS100" measured at 300 K and 15 K is less than ±2% of the total XMCD asymmetry $\Delta_{max,15\ K}$ at 15 K. For Co an unaltered XMCD asymmetry is not surprising, because only one chemical state of Co is found at the interface and in the bulk. For Mn the situation is different, because metallic Mn as well as MnO is present at the interface, but only metallic Mn in the bulk. Bulk MnO is antiferromagnetic with a critical temperature of $T_N=118$ K.[22] Therefore, at room temperature only metallic Mn can contribute to the XMCD asymmetry. For high spin Mn^{2+} ions in MnO the peaks in the calculated XMCD asymmetry[23] are found at nearly the same energies as the multiplet peaks "A1"–"B2" in the XAS spectrum. The energy positions of these peaks are marked by black vertical lines in Fig. 6(c). Obviously, the XMCD signal corresponding to metallic Mn peaks at *different* photon energies than for the Mn^{2+} ions. Therefore, a net magnetic moment of Mn^{2+} ions ferromagnetically exchange coupled to the ferromagnetic Co_2MnSi phase would change the shape of the XMCD asymmetry. This is not the case and, accordingly, the majority of the interfacial Mn^{2+} ions remains paramagnetic or becomes antiferromagnetically ordered at low temperature. Therefore, the generally larger temperature dependence of the Mn magnetic moment can be attributed to the metallic Mn in not perfectly ordered Co_2MnSi and might be a result of the antiferromagnetic Mn-Mn coupling in the alloy.

Finally, we note that the atomic ordering induced by the *in-situ* annealing process is not only reflected by the considerably increased magnetic moments, but also in differences of the spectral shape of the XMCD asymmetry [see inset in Fig. 6(c)]. This reflects changes of the electronic structure *above the Fermi level* E_F because of the thermally induced atomic ordering. Coexisting changes of the valence band states *below* E_F are shown in Sec. III E, after discussing the temperature dependence of the interfacial magnetization of Co and Fe in the Co-Fe-B based junctions.

D. Magnetic properties of Co and Fe in Co-Fe-B based junctions

In contrast to the best ordered sample "CMS100," where the Co (Mn) magnetic moments at room temperature are 94% (90%) of the low temperature values, the temperature dependence of the interfacial magnetic moments of sample "CoFeB" is weaker. Both, Co and Fe magnetic moments at the Co-Fe-B/AlO_x interface are only reduced to 98% (97%) of the low temperature moments, when the temperature increases from 25 K to 300 K. Therefore, thermal magnon excitation at the barrier/electrode interface is much more pronounced in the Co_2MnSi based junctions than in our MTJs

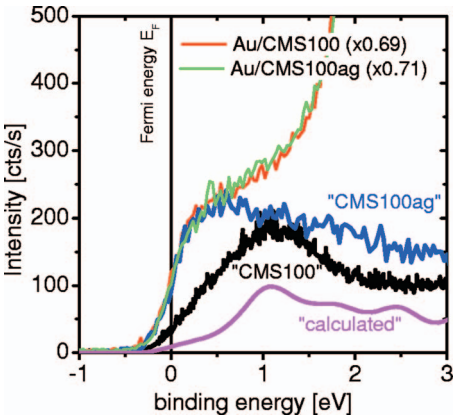

FIG. 7. (Color) Valence band spectra of the disordered and ordered samples "CMS100ag" and "CMS100," respectively. The valence band spectrum intensities of the 20 nm thick Au films covering one-half of the surfaces of both samples are scaled by a factor of 0.69 (Au on top of "CMS100") and 0.71 (Au on top of "CMS100ag"), respectively. The measurements were performed at room temperature. The lowest curve "calculated" shows the calculated density of occupied states for bulk Co_2MnSi (see text).

with Co-Fe-B electrodes. The possible influence of the enhanced magnon excitation on the transport properties of the $Co_2MnSi/AlO_x/Co_{70}Fe_{30}$ junctions is discussed in Sec. III F.

E. Electronic structure of Co_2MnSi based junctions

Complementary to the changes of the electronic band structure above E_F found in the XAS and XMCD spectra, we performed XPS measurements in the valence band range of "CMS100" and "CMS100ag." The binding energy scale of these XPS measurements of sample "CMS100" and "CMS100ag" was calibrated with respect to an internal Au reference. For this, one-half of each of both samples was covered by a 20 nm thick Au film prior to the measurements. The valence band spectra of "CMS100" and "CMS100ag" are shown in Fig. 7. As expected, the spectra of the two 20 nm thick Au reference films on "CMS100" and "CMS100ag" are identical. Only Au-$6s_{1/2}$ electrons are present at the Fermi energy E_F. The broadening of the Au Fermi edge corresponds to a total energy resolution of 350 meV. Around the Fermi energy E_F the valence band spectrum of the disordered sample "CMS100ag" coincides with the Au valence band spectrum, then a maximum intensity is found for binding energy E_B around 0.6 eV, followed by a slow intensity decrease for larger E_B. For the ordered sample "CMS100" the slope of the valence band spectrum close to E_F is considerably smaller than for Au and "CMS100ag." The intensity right at E_F is only 20% of the maximum intensity, which is found at $E_B=1.15$ eV. The insulating AlO_x barrier at the surface of "CMS100" and "CMS100ag" does not have electronic states at E_F, its gap energy is about 7 eV. Therefore, for $E_B \leqslant 3$ eV the valence band spectra of both samples are dominated by the Co_2MnSi valence states. For alloys containing the 3*d*-transition metals Co and Mn the valence band is dominated by their 3*d* electrons. Because our measurements are not spin resolved, the valence band spectra correspond mainly to the sum of the occupied majority and minority 3*d* states. Obviously, the maximum of the 3*d* density of states below E_F is found close to E_F for the disordered sample "CMS100ag," whereas for the ordered sample "CMS100" the most 3*d* states are found about 1 eV below E_F. The latter is in qualitative agreement with the band structure calculations: The lowest curve shown in Fig. 7 corresponds to the calculated spin-integrated total density of states, multiplied by the Fermi distribution function and convolved with a Gaussian distribution to account for the experimental resolution of 350 meV.

Finally we mention that atomic ordering leads to a small chemical shift of the Co-2*p* core levels: For the as-grown sample "CMS100ag" the Co-$2p_{3/2}$ binding energy measured by monochromated XPS is 778.2 eV (the Au $4f_{7/2}$ binding energy was set to 84.0 eV (Ref. 24)], which is close to the reference binding energy for pure Co (Ref. 24) (778.1 eV). For the ordered sample "CMS100" we observed a shift of 100 ± 50 mV to larger binding energies.

F. Influence of the electronic and magnetic interface properties on the transport properties

Now we discuss the transport properties of our Co_2MnSi based MTJs with respect to their chemical and magnetic interface properties presented in Secs. III B–III E.

The superparamagnetic behavior of the Co_2MnSi electrode found in the major loops of "CMS100ag" junctions (Fig. 1) is consistent with the temperature-dependent magnetic properties at the Co_2MnSi/AlO_x interface (Sec. III C). Especially, the superparamagnetism of the electrode can reduce its interfacial magnetization at ±2 kOe with raising temperature so strongly, that the TMR vanishes nearly at room temperature.

The considerably larger area resistance product in the "CMS100" and "CMS100ag" junctions compared to "CoFeB" and "MTJ-NiFe" is reasonable, although the exact atomic distribution of the Mn- and Si-oxide detected at the lower barrier interface cannot be extracted from our XAS measurements. Both oxides are insulators with gap energies of about 8 eV (SiO_2) and 3.6 eV [MnO (Ref. 22)] which should increase the effective barrier thickness for the tunneling electrons and, therefore, increase the resistance. Furthermore, a steplike tunnel barrier can account for an asymmetric differential tunneling characteristic as observed for "CMS100" as well as for "CMS100ag" [Fig. 1(b)]. The very similar tunneling characteristic for both types of Co_2MnSi based junctions further suggests, that their barrier shapes are comparable, too. This fact will be important for the discussion of the TMR inversion below.

In general, the temperature and bias voltage dependent transport properties of MTJs are rather complex because of the variety of different contributions to the total conductance like direct tunneling including band structure effects[25,26] and the shape of the tunnel barrier,[27] thermally induced changes of the interfacial magnetization,[28] magnon[29–31] and phonon assisted tunneling,[30] unpolarized conductance via defect states in the barrier,[28,32] spin scattering on paramagnetic ions in the barrier[33,34] and possible spin-flip scattering on interfacial antiferromagnons[34] in the MnO.

Because of the MnO formation at the lower barrier interface spin scattering on paramagnetic Mn^{2+} ions in the barrier[33,34] must be taken into account. For the small applied magnetic fields in our transport measurements ($\leqslant 0.2$ T) the Zeeman energy of paramagnetic Mn ions is much smaller than the smallest thermal energy ($k_B T \approx 1$ meV at 10 K) and bias voltage (1 mV). Accordingly, spin scattering on paramagnetic ions is a quasielastic process on our energy scale and should not influence the bias voltage or temperature dependence.[34] However, this process can reduce the effective spin polarization of the Co_2MnSi, which is indeed $P_{Co_2MnSi} = 66\%$ for the *in-situ* annealed "CMS100" junctions instead of theoretically expected 100%. The same holds for the unpolarized conductance via one defect state in the barrier,[32] which can partly reduce the effective polarization but does not have an influence on the bias voltage or temperature dependence. Please note, that the partial oxidation of Mn and Si at the barrier interface should disturb the ordering process of the interfacial Co_2MnSi during the *in-situ* annealing which should also contribute to the reduction of the effective spin-polarization of the Co_2MnSi.

The temperature-dependent XAS and XMCD data in Sec. III C shows no sign of a ferromagnetic coupling of Mn^{2+} ions to the atomically ordered Co_2MnSi at low temperature, but an antiferromagnetic ordering in the MnO at low temperature can be expected. As shown by Guinea[34] in first-order approximation spin-flip scattering on interfacial antiferromagnons should result in a decrease of the TMR with the square of the bias voltage. Phonon assisted tunneling[30] and unpolarized hopping conductance via two or more defect states[32] should also result in a nonlinear bias voltage dependence of the TMR. In contrast, a linear bias voltage dependence has been predicted for magnon assisted tunneling[30,31] assuming an energy independent band structure around the Fermi energy and surface magnon excitation. As pointed out in Sec. III A and shown in Fig. 8(a) in more detail such a linear bias voltage dependence of the TMR is indeed observed for the Co_2MnSi based junctions in the bias voltage (V) range of a few 10 mV. Compared with "CoFeB" and "MTJ-NiFe" junctions TMR(V) is considerably larger (within this model the small zero bias anomaly mentioned in Sec. III A is also explained by the magnon excitation). This would imply, that the magnon assisted tunneling is more pronounced in "CMS100" junctions. That is consistent with the temperature-dependent XAS and XMCD investigations which showed, that thermal magnon excitation is considerably larger at the Co_2MnSi/AlO_x than at the Co-Fe-B/AlO_x interface.

In general, we cannot rule out any influence on the TMR(V) behavior for small bias voltages by other current contributions (each leading to a nonlinear bias voltage dependence) or a bias voltage dependence of the effective spin polarization because of the electrodes' band structure. The latter can occur, when the spin-resolved densities of states in the electrodes change with energy, and in fact, it will become important for explaining the inverse TMR for large negative bias below. However, please note that if the bias voltage dependence is not governed by magnon excitation, the linear bias voltage dependence with maximal spin polarization at zero bias occurs just by accident. Additionally to the linear bias voltage dependence, the convex TMR temperature dependence of "CMS100" junctions is a characteristic feature for magnon-assisted tunneling as proposed by Han *et al.*[31] Taking only direct and magnon-assisted tunneling into account the resulting self-consistent fits (see Appendix A) of the bias voltage dependence of the TMR and the temperature dependence of the area resistance product for parallel (R^P) and antiparallel (R^{AP}) alignment as shown in Fig. 8(b) are very good. Especially, the best fit is found for antiparallel alignment of the Co_2MnSi and Co-Fe electrodes, when magnon-assisted tunneling would be most important. Please note, that the concave TMR temperature dependence of "MTJ-NiFe" (see Sec. III A, the same is found for MTJ "CoFeB") could not be reproduced by taking *only* direct and magnon-assisted tunneling into account.[9] Therefore, from the comparison of the transport properties and the temperature-dependent interfacial magnetic moments we suggest, that the TMR temperature and (low) bias voltage dependence of our *in-situ* annealed "CMS100" junctions is stronger compared with conventional Co-Fe-B or Co-Fe/Ni-Fe based MTJs because of enhanced magnon-assisted tunneling.

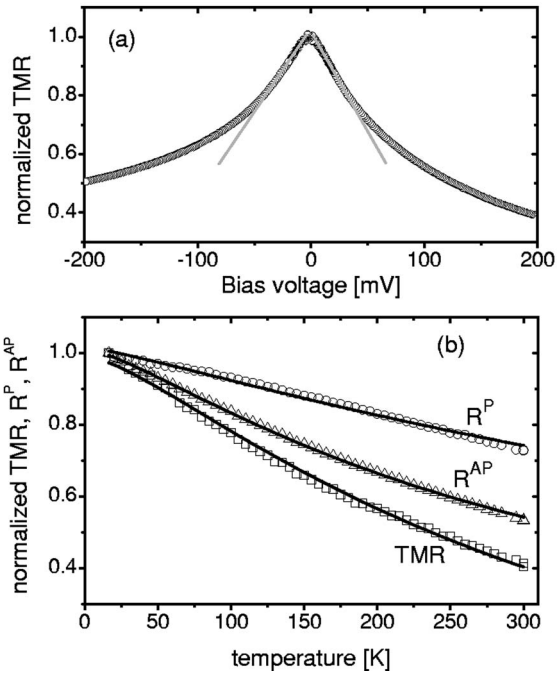

FIG. 8. (a) Typical normalized TMR bias voltage dependence of an *in situ* annealed "CMS100" junction around zero bias, measured at 16 K. (b) Typical temperature dependence of the normalized zero bias TMR, R^P and R^{AP} measured with two-probe ac technique (0.7 mV amplitude). The experimental data can be well reproduced by the magnon-assisted tunneling model (solid lines) proposed by Han *et al.* (Ref. 31).

Finally, the inversion of the TMR for larger bias voltage is an astonishing feature. A bias voltage dependent inversion of the TMR has been reported for $La_{0.7}Sr_{0.3}MnO_3/SrTiO_3/Co$ MTJs by De Teresa *et al.*,[35] for Fe/MgO/Fe MTJs by Tiusan *et al.*,[36] for Co/Al-O/Co MTJs by Montaigne *et al.*,[27] for Ni-Fe/Ta-O/Al-O/Ni-Fe by Sharma *et al.*[37] and has also been recently observed for Al-O based junctions with Co_2FeSi single layer and Co_2MnSi/Co_2FeSi multilayer elec-

trode by our group.[38] The effective spin polarization of the tunneling electrons does not only depend on the band structure of the electrode but also on the barrier material[35] and structure[39] used in the experiment. Especially, for AlO_x based junctions with transition metal (or alloy) electrodes the spin polarization of the tunneling electrons was found to be always positive[40] in case of small bias voltages. This was interpreted as a favored tunneling of electrons with *s*-character[35,41] hybridized with *d* electrons. In case of MTJs not based on single Al-O barriers the authors[35–37] have related the bias voltage dependent inversion of the TMR to the band structure of the electrodes. In contrast, Montaigne *et al.*[27] and de Buttet *et al.*[42] pointed out, that even for a simple free-electron-like model with parabolic band structure a complex TMR(V) dependence (including inversion of the TMR) can be calculated, if a certain shape of the barrier is present and if electrons with nonvanishing wave-vector component parallel to the barrier contribute to the current.

However, as we will discuss in the following we suggest, that the TMR inversion is a band structure effect in the case of Al-O based MTJs with an ordered Co_2MnSi electrode. Within the calculations by Montaigne *et al.*[27] and de Buttet *et al.*[42] a certain shape of the TMR bias voltage dependence, e.g., an inversion only for one bias voltage direction, is always connected to a certain asymmetry of the current-voltage characteristic. But although the tunneling characteristics and the resistances of "CMS100ag" and "CMS100" are very similar (Sec. III A), *only* the annealed sample "CMS100" with atomically ordered Co_2MnSi electrode shows an inversion of the TMR for large negative bias. Furthermore, our XAS, XMCD, and XPS investigations presented in Sec. III C and III E revealed significant differences of the band structure of "CMS100" and "CMS100ag" which are consistent with the band structure calculations. Finally, the observed TMR inversion is consistent with calculations of the spin polarization of the tunneling electrons in ordered Co_2MnSi: According to the above-mentioned favored tunneling of *s* electrons in case of Al-O barriers, we assume that tunneling of *s* electrons also dominates in our junctions. The monotonic decrease of the TMR with increasing bias voltage of our "CoFeB," "CMS100ag," and "MTJ-NiFe" junctions without changing the sign of the TMR just reflects the fact that the sign of the bias voltage-dependent effective spin polarization of the *s*-electrons does not change. The density of states in $L2_1$-ordered Co_2MnSi is dominated by the $\uparrow$ (majority)- and $\downarrow$ (minority)-3*d* electrons of Co and Mn.[5,13] Because of exchange interaction between these electrons and *s* electrons, important features of the density of states for $\uparrow$- and $\downarrow$-3*d* electrons are also reflected by the spin-dependent *s*-electron density of states. Using Julliére's definition[3] of the effective spin polarization the expected energy dependent polarization of the *s* electrons can be calculated as $P(E)_s = [N(E)_s^{\uparrow} - N(E)_s^{\downarrow}]/[N(E)_s^{\uparrow} + N(E)_s^{\downarrow}]$, where $N(E)_s^{\uparrow,\downarrow}$ are the density of the majority and minority *s* electrons, respectively, calculated by the SPR-KKR code.[11] The result is shown in Fig. 9. While $P(E)_s$ is positive for the occupied states of interest, it changes its sign above E_F. Please note, that the polarization is close to 100% around and below E_F. This corresponds to a very low density of states for the minority *s* electrons (the same holds for *p* and *d* electrons). A real gap in the minority channel of all electrons as predicted by Ishida *et al.*[5] has not been found in our calculations, but the calculated $P(E)_s$ can explain the strong asymmetric bias voltage dependence of our *in-situ* annealed "CMS100" junctions. For positive bias the electrons may tunnel *from occupied positively polarized s*-like states in Co_2MnSi just below E_F *into unoccupied positively polarized s*-like states in Co-Fe. For negative bias the situation is reversed, the electrons can tunnel *from occupied positively polarized s*-like states in Co-Fe just below E_F *into unoccupied negatively polarized s*-like states in Co_2MnSi. Because of the energy integration in the tunneling current for a certain bias voltage *V*, which corresponds to a bias voltage-dependent averaging of $P(E)_s$, the TMR becomes not immediately negative, when $|V|$ becomes larger than 0.25 V. However, as mentioned above a kink in the bias voltage dependence around $V=-0.3$ V is observed (see arrow in Fig. 3). For the "CMS100ag" junctions prepared without *in-situ* annealing this inversion of the effective spin polarization of tunneling electrons does not take place.

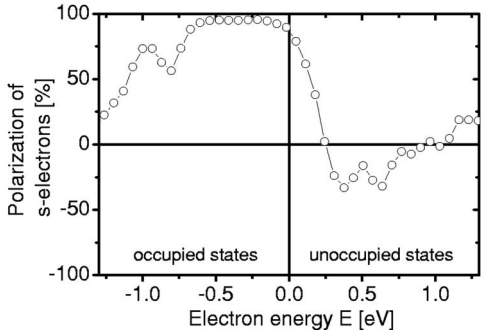

FIG. 9. Energy dependence of the effective spin polarization for *s* electrons in perfectly ordered bulk Co_2MnSi calculated by the SPR-KKR code (Ref. 11).

IV. CONCLUSION

We presented investigations on the structural and transport properties of Al-O based magnetic tunnel junctions with Co_2MnSi electrode and compared their properties with more standard MTJs with Ni-Fe/Co-Fe as well as with Co-Fe-B electrodes. The investigation of the temperature-dependent magnetic and chemical properties of the Co_2MnSi/AlO_x interface in the Co_2MnSi based MTJs showed, that with increasing degree of disorder, interfacial magnetic moments are reduced and their temperature dependences are more pronounced. Magnon excitation is stronger at the Co_2MnSi/AlO_x interface compared with Co-Fe-B based tunnel junctions and bulk Co_2MnSi. We suggest, that mainly this contributes to the larger bias voltage and temperature dependence of the TMR in the Co_2MnSi based junctions by means of enhanced magnon-assisted tunneling. Furthermore, several fingerprints of the ideal Co_2MnSi band structure of atomically ordered Co_2MnSi films are revealed by the XAS-, XMCD-, and XPS investigations in accordance with SPR-KKR calculations. Finally, we suggest that the observed inversion of the TMR effect occuring when electrons are

tunneling from the Co-Fe into the atomically ordered Co_2MnSi electrode is the most striking band structure effect.

ACKNOWLEDGMENT

Financial support by the Deutsche Forschungsgemeinschaft (DFG) and valueable help by A. T. Young is gratefully acknowledged. The Advanced Light Source is supported by the U.S. Department of Energy under Contract No. DE-AC03-76SF00098.

APPENDIX: SELF-CONSISTENT FIT OF THE BIAS VOLTAGE AND TEMPERATURE DEPENDENCE OF THE TMR

The magnon-assisted tunneling model by Han *et al.*[31] takes only direct and magnon-assisted tunneling into account to explain the bias voltage *and* the temperature dependence of the TMR self-consistently. The model was originally deduced for MTJs with identical ferromagnetic electrodes. Because this assumption is a simplification of our system, all fitting parameters must be interpreted as effective parameters representing the average of the parameters for the individual electrodes. According to this model, the bias voltage dependence of the TMR at low temperature and small bias is fitted first by the following equation [Eq. (17) in Ref. 31]:

$$\mathrm{TMR}_{T\simeq 0}(V) = \mathrm{TMR}_{T\simeq 0}(V\simeq 0) - \frac{R^{AP}_{T\simeq 0}(V\simeq 0)}{R^{P}_{T\simeq 0}(V\simeq 0)}\left(\frac{1}{\xi}-\xi\right)\frac{QSeV}{E_m}. \quad \text{(A1)}$$

For detailed information on the definition of all parameters we refer to Ref. 31, here we mention their physical meaning: $R^{AP,P}_{T\simeq 0}(V\simeq 0)$ are the area resistance products for antiparallel and parallel alignment of the electrodes in the limit of low temperature T and nearly zero bias voltage V. ξ is connected to the effective spin polarization of the MTJ and can be calculated from the TMR amplitude $\mathrm{TMR}_{T\simeq 0}(V\simeq 0)$ at low temperature and nearly zero bias voltage. For the junction shown in Fig. 8 we obtain $\xi=0.548$. e is the electron charge. S is the spin quantum number and E_m characterizes the magnon dispersion relation of the FM, it is proportional to its Curie temperature. Q describes essentially the ratio of the matrix elements for direct and magnon-assisted tunneling. The free fitting parameter of the bias voltage dependence is the quantity QS/E_m. We performed the fit for positive and negative bias voltage [grey lines in Fig. 8(a)] and got the average value of $QS/E_m=1.38\times 10^{19}\ \mathrm{J}^{-1}$. This is about 3 times larger than the results of Han *et al.*[31] for Co-Fe/Al-O/Co-Fe. Within this model this means, that magnon assisted tunneling is more important for our Co_2MnSi based junction than for the more standard junctions with Co-Fe electrodes.

The next step is to fit the temperature dependence of the area resistance products $R^{AP,P}_{V\simeq 0}(T)$ at nearly zero bias for parallel and antiparallel alignment [Eqs. (18) and (19) in Ref. 31] with the following fitting function:

$$R^{AP}_{V\simeq 0}(T) = R^{AP}_{V=0}(T=0)[1+(Q/\xi)(2Sk_BT/E_m)\ln(k_BT/E^{AP}_C)]^{-1}, \quad \text{(A2)}$$

$$R^{P}_{V\simeq 0}(T) = R^{P}_{V=0}(T=0)[1+Q\xi(2Sk_BT/E_m)\ln(k_BT/E^{P}_C)]^{-1}. \quad \text{(A3)}$$

$E^{AP,P}_C$ are the anisotropic-cutoff energies for the different magnetic configurations. Each fit is performed with two free parameters, namely $R^{AP,P}_{V=0}(T=0)$ and $E^{AP,P}_C$. We obtain $R^{AP}_{V=0}(T=0)=265.1\pm 0.4\ \mathrm{k\Omega}$ and $R^{P}_{V=0}(T=0)=146.7\pm 0.4\ \mathrm{k\Omega}$, naturally both values are very close to the experimental values of 263.2 kΩ and 144.4 kΩ measured at 16 K with 0.7 mV ac bias voltage. The extracted cutoff energies are $E^{P}_C=72\pm 7\ \mu\mathrm{V}$ and $E^{AP}_C=428\pm 9\ \mu\mathrm{V}$. As also found by Han *et al.*[31] for $Co_{75}Fe_{25}$/Al-O/$Co_{75}Fe_{25}$ junctions, both cutoff energies are in the energy range of a few 100 μV and $E^{AP}_C > E^{P}_C$.

*Electronic address: jschmalh@physik.uni-bielefeld.de

[1] S. A. Wolf, D. D. Awschalom, R. A. Buhrman, J. M. Daughton, S. von Molnar, M. L. Roukes, A. Y. Chtchelkanova, and D. M. Treger, Science **294**, 1488 (2001).

[2] G. Reiss and D. Meyners, Appl. Phys. Lett. **88**, 043505 (2006).

[3] M. Julliere, Phys. Lett. **54A**, 225 (1975).

[4] S. Ikeda, J. Hayakawa, Y. M. Lee, R. Sasaki, T. Meguro, F. Matsukura, and H. Ohno, Jpn. J. Appl. Phys., Part 2 **44**, L1442 (2005).

[5] S. Ishida, T. Masaki, S. Fujii, and S. Asano, Physica B **245**, 1 (1998).

[6] J. Schmalhorst, S. Kämmerer, G. Reiss, and A. Hütten, Appl. Phys. Lett. **86**, 152102 (2005).

[7] S. Kämmerer, S. Heitmann, D. Meyners, D. Sudfeld, A. Thomas, A. Hütten, and G. Reiss, J. Appl. Phys. **93**, 7945 (2003).

[8] M. Oogane, Y. Sakuraba, J. Nakata, H. Kubota, Y. Ando, A. Sakuma, and T. Miyazaki, J. Phys. D **39**, 834 (2006).

[9] J. Schmalhorst and G. Reiss, Phys. Rev. B **68**, 224437 (2003).

[10] Y. U. Idzerda, C. T. Chen, H.-J. Lin, G. Meigs, G. H. Ho, and C.-C. Kao, Nucl. Instrum. Methods Phys. Res. A **347**, 134 (1994).

[11] The Munich SPR-KKR package, version 2.1.3, H. Ebert *et al.*, http://olymp.cup.uni-muenchen.de/ak/ebert/SPRKKR; H. Ebert, "Fully relativistic band structure calculations for magnetic solids—Formalism and application," in *Electronic Structure and Physical Properties of Solids*, edited by H. Dreysse, Lecture Notes in Physics, Vol. 535, (Springer, Berlin), p. 191.

[12] S. Schuppler, S. L. Friedman, M. A. Marcus, D. L. Adler, Y.-H. Xie, F. M. Ross, T. D. Harris, W. L. Brown, Y. L. Chabal, L. E. Brus *et al.*, Phys. Rev. Lett. **72**, 2648 (1994).

[13] I. Galanakis, P. H. Dederichs, and N. Papanikolaou, Phys. Rev. B **66**, 174429 (2002).

[14] Y. Yonamoto, T. Yokoyama, K. Amemiya, D. Matsumura, and T. Ohta, Phys. Rev. B **63**, 214406 (2001).

[15] C. T. Chen, Y. U. Idzerda, H.-J. Lin, N. V. Smith, G. Meigs, E. Chaban, G. H. Ho, E. Pellegrin, and F. Sette, Phys. Rev. Lett.

75, 152 (1995).
[16] I. Galanakis (private communication); the given numbers of 3*d* holes based on the work of Galanakis *et al.* (Ref. 13).
[17] J. Schmalhorst, S. Kämmerer, M. Sacher, G. Reiss, A. Hütten, and A. Scholl, Phys. Rev. B **70**, 024426 (2004).
[18] H. Ohldag, A. Scholl, F. Nolting, E. Arenholz, S. Maat, A. T. Young, M. Carey, and J. Stöhr, Phys. Rev. Lett. **91**, 017203 (2003).
[19] P. Langevin, Ann. Chim. Phys. **5**, 70 (1905).
[20] S. Picozzi, A. Continenza, and A. J. Freeman, Phys. Rev. B **69**, 094423 (2004).
[21] L. Ritchie, G. Xiao, Y. Ji, T. Y. Chen, C. L. Chien, M. Zhang, J. Chen, Z. Liu, G. Wu, and X. X. Zhang, Phys. Rev. B **68**, 104430 (2003).
[22] P. A. Cox, *Transition Metal Oxides, Table 3.6* (Clarendon, Oxford, 1992).
[23] G. van der Laan and B. T. Thole, Phys. Rev. B **43**, 13401 (1991).
[24] A. Thomson, D. Attwood, E. Gullikson, M. Howells, J. Kortright, A. Robinson, J. Underwood, K.-J. Kim, J. Kirz, I. Lindau *et al.*, X-ray data booklet, Lawrence Berkeley National Laboratory, http://xdb.lbl.gov
[25] E. L. Wolf, *Principles of Electron Tunneling Spectroscopy* (Oxford University Press, Oxford 1989).
[26] A. M. Bratkovsky, Phys. Rev. B **56**, 2344 (1997).
[27] F. Montaigne, M. Hehn, and A. Schuhl, Phys. Rev. B **64**, 144402 (2001).
[28] C. H. Shang, J. Nowak, R. Jansen, and J. S. Moodera, Phys. Rev. B **58**, R2917 (1998).
[29] S. Zhang, P. M. Levy, A. C. Marley, and S. S. P. Parkin, Phys. Rev. Lett. **79**, 3744 (1997).
[30] A. M. Bratkovsky, Appl. Phys. Lett. **72**, 2334 (1998).
[31] X.-F. Han, A. C. C. Yu, M. Oogane, J. Murai, T. Daibou, and T. Miyazaki, Phys. Rev. B **63**, 224404 (2001).
[32] Y. Xu, D. Ephron, and M. R. Beasley, Phys. Rev. B **52**, 2843 (1995).
[33] R. Jansen and J. S. Moodera, Phys. Rev. B **61**, 9047 (2000).
[34] F. Guinea, Phys. Rev. B **58**, 9212 (1998).
[35] J. M. De Teresa, A. Barthélémy, A. Fert, J. P. Contour, R. Lyonnet, F. Montaigne, P. Seneor, and A. Vauèr Phys. Rev. Lett. **82**, 4288 (1999).
[36] C. Tiusan, J. Faure-Vincent, C. Bellouard, M. Hehn, E. Jouguelet, and A. Schuhl, Phys. Rev. Lett. **93**, 106602 (2004).
[37] M. Sharma, S. X. Wang, and J. H. Nickel, Phys. Rev. Lett. **82**, 616 (1999).
[38] D. Ebke, J. Schmalhorst, N.-N. Liu, A. Thomas, G. Reiss, and A. Hütten, Appl. Phys. Lett. (to be published).
[39] A. Thomas, J. S. Moodera, and B. Satpati, J. Appl. Phys. **97**, 10C908 (2005).
[40] R. Meservey and P. M. Tedrow, Phys. Rep. **238**, 173 (1994).
[41] J. A. Hertz and K. Aoi, Phys. Rev. B **8**, 3252 (1973).
[42] C. de Buttet, M. Hehn, F. Montaigne, C. Tiusan, G. Malinowski, A. Schuhl, E. Snoeck, and S. Zoll, Phys. Rev. B **73**, 104439 (2006).